Optics Letters

Measuring different types of transverse momentum correlations in the biphoton's Fourier plane

Omar Calderón-Losada,* Jefferson Flórez, Juan P. Villabona-Monsalve, and Alejandra Valencia

Laboratorio de Óptica Cuántica, Universidad de los Andes, A.A. 4976, Bogotá D.C., Colombia
**Corresponding author: o.calderon31@uniandes.edu.co*

Received 18 December 2015; revised 10 February 2016; accepted 11 February 2016; posted 11 February 2016 (Doc. ID 255830); published 8 March 2016

In this Letter, we present a theoretical and experimental study about the spatial correlations of paired photons generated by Type II spontaneous parametric down-conversion. In particular, we show how these correlations can be positive or negative, depending on the direction in which the far-field plane is scanned and the polarization postselected. Our results provide a straightforward way to observe different kind of correlations that complement other well-known methods to tune the spatial correlations of paired photons.

OCIS codes: (190.4420) Nonlinear optics, transverse effects in; (190.4975) Parametric processes; (270.5290) Photon statistics.

http://dx.doi.org/10.1364/OL.41.001165

Correlations have played an important role in fundamental physics and practical applications. Regarding fundamental issues, it was precisely the fact that quantum mechanics allows the existence of the strong correlation, called entanglement, that motivated the discussions between Einstein and Bohr in the first years of quantum physics [1]. In the 1970s, the possibility of measuring correlations between different locations enabled the experimental demonstration of entanglement, revealing in this way new features of nature [2].

Besides the fundamental physical implications behind correlations, they have become a convenient tool for practical applications. For example, the feature of nonlocality derived from entanglement appears as a suitable element for remote applications. In particular, using the continuous time/frequency variables, the possibility of performing remote spectrometry and different protocols for clock synchronization have been developed [3,4]. Also, in the spatial case, experiments such as quantum imaging, quantum interference, and quantum lithography have been presented [5–8]. Furthermore, regarding discrete variables, polarization entanglement has allowed the use of teleportation in quantum information tasks [9].

Since the 1980s, the nonlinear optical process of spontaneous parametric down conversion (SPDC) has provided a convenient source of entangled photon pairs [10]. Interestingly, due to the intrinsic nature of the SPDC process, the generated photons are entangled in the temporal [11], spatial [12], and polarization degrees of freedom [13]. The models developed so far, to describe the SPDC process, suit with the experimental results for the spectral correlations very well [14,15]. Regarding the spatial domain, several authors have reported on the dependence of the spatial correlations on crystal's length, pump's waist, geometry of the down-converted process, and even different combinations of the transverse spatial variables [16–20]. More recently, the implementation of a new family of sensitive CCD cameras has allowed researchers to revisit and study such spatial correlations [21,22], not only in SPDC but also in the high-gain regime [23,24]. All these interesting results have been presented for Type I phase matching. On the other hand, for photons generated by noncollinear Type II SPDC, there has been less experimental work. For example, in Ref. [25] the position and transverse momentum correlations of photon pairs have been measured in order to study spatial entanglement. Although in this Letter the authors used a Type II crystal, the effects of the different polarizations between signal and idler on the spatial correlations are lost because the setup used combines the SPDC output with a two-photon interferometer.

In the present work, we report the measurement of the transverse momentum correlation for noncollinear Type II SPDC pairs as they come out directly from the crystal. As a remarkable result, we find different kind of transverse correlations between photons when we scan in perpendicular directions in the Fourier plane and use different postselection schemes. These experimental results provide a direct way to have different kinds of correlations that complement other well-known methods to tune them. Additionally, it could be used to generated a counter-Einstein–Podolsky–Rosen (CEPR) state that has positive correlation in transverse momentum and a negative correlation (anticorrelation) in position [26].

The physical phenomena studied here are depicted in Fig. 1: Photons generated by SPDC and that travel by the intersections of the two cones, as can be seen in the inset, are collected by two detection systems placed in the Fourier plane of the

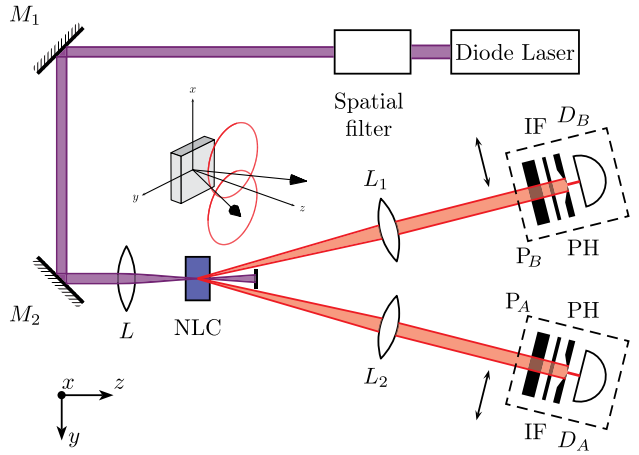

Fig. 1. Experimental setup. The diode laser has a central wavelength at 407 nm and is spatially shaped as a Gaussian beam with a waist of 31 μm and 42 μm in the horizontal (y-direction) and vertical (x-direction) direction, respectively. M_1 and M_2 are mirrors. L is a lens with focal length of 150 mm that fixes the desired waist on the 4-mm BBO Type II crystal (NLC) cut at 44.5° to generate a pair of down-converted photons at a half-open angle of ∼6°. Each lens L_1 and L_2, both with focal lengths of 750 mm, configures a $2f$-system. The detection system consists of a polarizer P_η, a 5 nm-bandwidth interference filter (IF) centered at 814 nm, a pinhole (PH) and a multimode fiber to take the photons to detectors, D_A and D_B.

crystal's output face in order to measure coincidences between the two detectors and reconstruct the spatial transverse correlation. For a Type II SPDC process, using first order perturbation theory and the paraxial approximation, the two-photon state as a function of the transverse wave vectors $\mathbf{q}_\mu = (q_\mu^x, q_\mu^y)$ and frequency detunings, $\Omega_\mu = \omega_\mu - \omega_0^\mu$, around the central frequencies, ω_0^μ, for the extraordinary (e) and ordinary (o) fields ($\mu = e, o$), is given by

$$|\psi\rangle = \int \mathrm{d}\mathbf{q}_e \mathrm{d}\mathbf{q}_o \mathrm{d}\Omega_e \mathrm{d}\Omega_o \times [\Phi(\mathbf{q}_e, \Omega_e; \mathbf{q}_o, \Omega_o)\hat{a}^\dagger(\Omega_e, \mathbf{q}_e)\hat{a}^\dagger(\Omega_o, \mathbf{q}_o) + \Phi(\mathbf{q}_o, \Omega_o; \mathbf{q}_e, \Omega_e)\hat{a}^\dagger(\Omega_e, \mathbf{q}_e)\hat{a}^\dagger(\Omega_o, \mathbf{q}_o)]|0\rangle, \quad (1)$$

where $\Phi(\mathbf{q}_e, \Omega_e; \mathbf{q}_o, \Omega_o)$ and $\Phi(\mathbf{q}_o, \Omega_o; \mathbf{q}_e, \Omega_e)$ are the mode functions or biphotons that contain all the information about the correlations between the pair of down-converted photons, and the operator $\hat{a}^\dagger$ indicates the creation of an μ-polarized photon with transverse momentum $\mathbf{q}_\mu$ and frequency detuning Ω_μ.

The mode function $\Phi(\mathbf{q}_e, \Omega_e; \mathbf{q}_o, \Omega_o)$ is related, with the joint probability of detecting both an e-polarized down-converted photon, with transverse momentum $\mathbf{q}_e$ and frequency detuning Ω_e, at detector A and an o-polarized photon, with transverse momentum $\mathbf{q}_o$ and frequency detuning Ω_o at detector B. An analogous definition applies for $\Phi(\mathbf{q}_o, \Omega_o; \mathbf{q}_e, \Omega_e)$. Particularly, $\Phi(\mathbf{q}_e, \Omega_e; \mathbf{q}_o, \Omega_o)$ reads

$$\Phi(\mathbf{q}_e, \Omega_e; \mathbf{q}_o, \Omega_o) = \mathcal{N}\alpha(\Delta_0, \Delta_1)\beta(\Omega_e, \Omega_o) \times \mathrm{sinc}\left(\frac{\Delta_k L}{2}\right) \exp\left(i\frac{\Delta_k L}{2}\right), \quad (2)$$

where $\mathcal{N}$ is a normalization constant, $\alpha(\Delta_0, \Delta_1)$ and $\beta(\Omega_e, \Omega_o)$ have the functional form of the pump's transverse and spectral distribution, respectively, L is the length of the nonlinear crystal, and Δ_0, Δ_1 and Δ_k are functions that result from the phase-matching conditions and are defined as

$$\Delta_0 = q_e^x + q_o^x, \quad (3a)$$

$$\Delta_1 = q_e^y \cos\phi_e + q_o^y \cos\phi_o - N_e\Omega_e \sin\phi_e + N_o\Omega_o \sin\phi_o - \rho_e q_e^x \sin\phi_e, \quad (3b)$$

$$\Delta_k = N_p(\Omega_e + \Omega_o) - N_e\Omega_e \cos\phi_e - N_o\Omega_o \cos\phi_o - q_e^y \sin\phi_e + q_o^y \sin\phi_o + \rho_p\Delta_0 - \rho_e q_e^x \cos\phi_e. \quad (3c)$$

The angles ϕ_e and ϕ_o are the creation angles of the down-converted photons inside the crystal with respect to the pump's propagation direction, whereas the angles ρ_p and ρ_e account for the walk-off of the pump (p) and the extraordinary down-converted photon, respectively. These last angles are given by $\rho_\epsilon = -\frac{1}{n_\epsilon}\frac{\partial n_\epsilon}{\partial \theta_\epsilon}$, ($\epsilon = p, e$), where n_ϵ is the effective refractive index and θ_ϵ is the angle formed by the corresponding wave vector and the optical axis of the nonlinear crystal. In this study, ϕ_e and ϕ_o are treated as constants, mainly because the scanned transverse momentum regions represent a small portion around the emission angles. $N_\mu = \frac{dn_\mu(\omega_\mu)\omega_\mu}{d\omega_\mu}|_{\omega_\mu=\omega_0^\mu}$ denotes the inverse of the group velocity for each photon.

A good way to grasp the information about the correlations that are contained in Eq. (2) is by taking into account the following considerations: A pump beam with a Gaussian profile with waist w_p in such a way that $\alpha(\Delta_0, \Delta_1) \propto \exp[-w_p^2(\Delta_0^2 + \Delta_1^2)/4]$, a CW pump laser, i.e., $\beta(\Omega_e, \Omega_o) \propto \delta(\Omega_e + \Omega_o)$, and the sinc function approximated by a Gaussian function with the same width at $1/e^2$ of its maximum, i.e., $\mathrm{sinc}(x) \approx \exp(-\gamma x^2)$ with γ equal 0.193. With these two considerations Eq. (2) reduces to

$$\Phi(\mathbf{q}_e, \Omega_e; \mathbf{q}_o, \Omega_o) = \mathcal{N}\beta(\Omega_e, \Omega_o) \times \exp\left[-\frac{w_p^2(\Delta_0^2 + \Delta_1^2)}{4} - \gamma\left(\frac{\Delta_k L}{2}\right)^2 + i\frac{\Delta_k L}{2}\right]. \quad (4)$$

In order to observe the transverse correlations, the frequency information has to be traced out, hence the spatial biphoton, $\tilde{\Phi}(\mathbf{q}_e; \mathbf{q}_o)$ is given by $\int \mathrm{d}\Omega_e \mathrm{d}\Omega_o f_e(\Omega_e) f_o(\Omega_o) \Phi(\mathbf{q}_e, \Omega_e; \mathbf{q}_o, \Omega_o)$, where $f_\mu(\Omega_\mu)$ represents the behavior of the spectral filters placed in front of each detector. For the present study, these filters are modeled as $f_\mu(\Omega_\mu) = \exp[-\Omega_\mu^2/(4\sigma_\mu^2)]$, with bandwidth σ_μ chosen to achieve a regimen where the spatial-spectral correlations are completely broken [27].

Experimentally, it is possible to obtain information about the spatial biphoton by measuring the rate of coincidence counts. For an e-photon with transverse momentum $\mathbf{q}_e$ at the detector A, and the o-photon with transverse momentum $\mathbf{q}_o$ at detector B such rate is given by

$$S(\mathbf{q}_e;\mathbf{q}_o) \equiv |\tilde{\Phi}(\mathbf{q}_e;\mathbf{q}_o)|^2 = \left| \int d\Omega_e d\Omega_o f_e(\Omega_e) f_o(\Omega_o) \Phi(\mathbf{q}_e,\Omega_e;\mathbf{q}_o,\Omega_o) \right|^2. \quad (5)$$

Analogously, the corresponding coincidence rate where the e-photon is detected at B and the o-photon is detected at A, is defined by $S(\mathbf{q}_o;\mathbf{q}_e) \equiv |\tilde{\Phi}(\mathbf{q}_o,\mathbf{q}_e)|^2$.

The theoretical predictions for the coincidence rates can be seen in the top panels of Figs. 2 and 3, where the biphoton $\Phi(\mathbf{q}_e,\Omega_e;\mathbf{q}_o,\Omega_o)$ is the one of Eq. (4), and additionally, it has been the fact that in the Fourier plane there is a one-to-one correspondence between the transverse momentum and position. Explicitly $\mathbf{q} = \frac{2\pi}{\lambda^0 f}\tilde{\mathbf{x}}$, and therefore

$$S(\mathbf{q}_e;\mathbf{q}_o) = \left| \tilde{\Phi}\left(\frac{2\pi}{\lambda_e^0 f}\tilde{\mathbf{x}}_A, \frac{2\pi}{\lambda_o^0 f}\tilde{\mathbf{x}}_B \right) \right|^2, \quad (6)$$

where λ_μ^0 is the central wavelength of the μ-polarized down-converted photon, $\tilde{\mathbf{x}}_\eta = (x_\eta, y_\eta)$ $(\eta = A, B)$ denotes a position vector in the biphoton's Fourier plane, and f is the focal length of a lens that is used to do the transformation to the Fourier plane in the experimental setup. Figs. 2(a) and 2(b) depict $S(q_e^y; q_o^y)$ and $S(q_o^y; q_e^y)$, respectively, showing the correlations in the y-direction between the two Fourier planes. On the other hand, Figs. 3(a) and 3(b) depict $S(q_e^x; q_o^x)$ and $S(q_o^x; q_e^x)$, respectively, showing the correlations in the x-direction. It is important to point out three remarkable observations. First, the y-transverse momentum exhibits a positive correlation, whereas the x-transverse momentum shows a negative one. This observation is interesting, since it tells us that just by performing a change in the scanning direction of the Fourier plane, it is possible to observe a completely different kind of spatial correlation. In other words, in a Type II SPDC process, both kinds of momentum correlations, positive and negative, are present, depending on the observed direction of the far-field plane. Second, the positive correlation present in the y-direction may be surprising at first sight, since one expects an anticorrelation for the transverse momentum of down-converted photons; however, this is true only for certain values of the pump's waist. The waist chosen to depict Fig. 2, $w_p = 31$ μm, is such that together with the other relevant parameters in the SPDC generation yields to a positive correlation. This is similar to what has been reported for the Type I case [17]. Third, the spatial correlation in the y-direction is insensitive to which polarization arrives to each detector. On the contrary, the spatial correlation in the x-direction is highly affected by the detected polarization, as is revealed by the different orientations of $S(q_e^x; q_o^x)$ and $S(q_o^x; q_e^x)$.

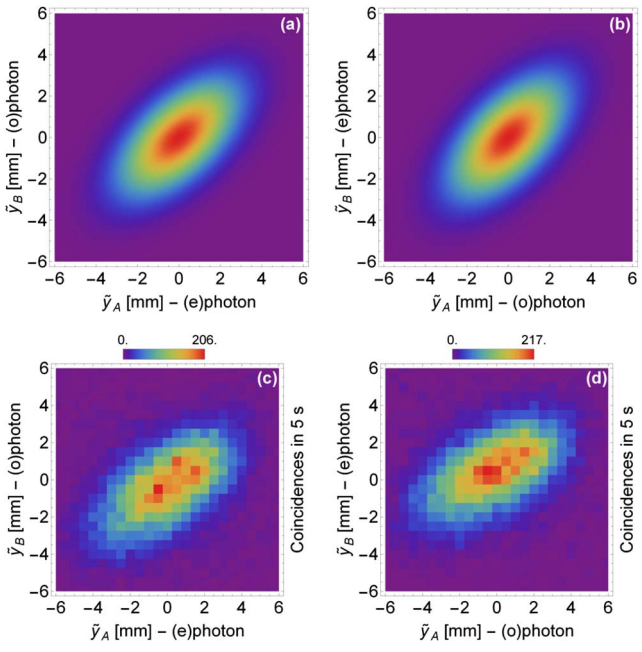

Fig. 2. Spatial correlations in the y-direction at the biphoton's Fourier plane. Panels (a) and (c) depict $S(q_e^y; q_o^y)$ from the theoretical model and the experimental results, respectively. Panels (b) and (d) depict $S(q_o^y; q_e^y)$ from the theoretical model and the experimental results, respectively.

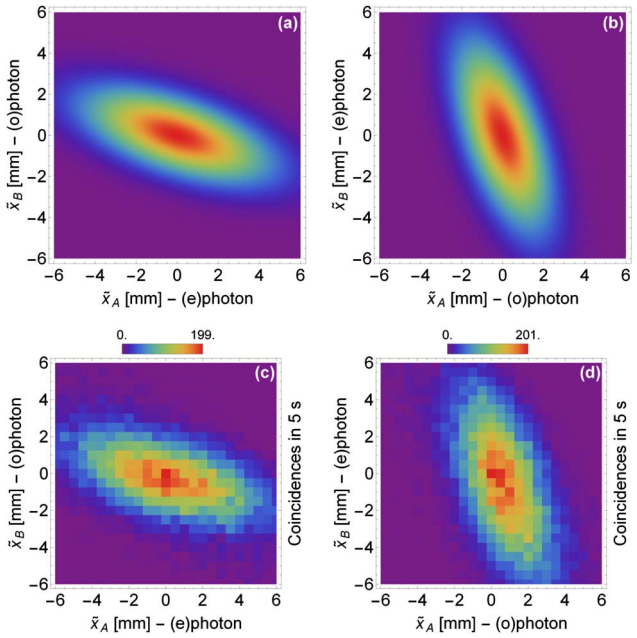

Fig. 3. Spatial correlations in the x-direction at the biphoton's Fourier plane. Panels (a) and (c) depict $S(q_e^x; q_o^x)$ from the theoretical model and the experimental results, respectively. Panels (b) and (d) depict $S(q_o^x; q_e^x)$ from the theoretical model and the experimental results, respectively.

To corroborate the previous theory, the setup in Fig. 1 is implemented, where a diode laser beam, centered at 407 nm, vertically polarized (e-polarized), and spatially shaped by a spatial filter, is focused by a lens L into a 4-mm-length Type II BBO (beta barium borate) crystal. Each of the generated down-converted photons passes through a $2f$-system in order to obtain the momentum distribution of the photon pairs at the Fourier plane. The combined scan to measure momentum correlations is accomplished by two detection systems that consist of polarizers, interference filters, 2.0 mm-diameter pinholes, multimode fibers and single photon counters (SPCM-AQRH-13), D_A and D_B, whose outputs are analyzed by a FPGA card that allows counting of singles and coincidences. The detection systems are mounted on automated translational stages to do a full scan of the biphoton's Fourier plane either in the horizontal or vertical direction. In the experiment, we

perform the measurement of $S(\mathbf{q}_e;\mathbf{q}_o)$ or $S(\mathbf{q}_o;\mathbf{q}_e)$ by rotating the polarizers, P_A and P_B, to detect either the *e*- or *o*-photon in the corresponding detector, D_A or D_B.

When both detectors are scanned in the direction parallel to the optical table (*y*-direction), the bottom panel in Fig. 2 shows the experimental results when postselecting different polarizations for each detector. In particular, Fig. 2(c) shows $S(q_e^y;q_o^y)$ and Fig. 2(d) shows $S(q_o^y,q_e^y)$. In both situations, the momentum correlation is in good agreement with the theory. On the other hand, the bottom panels of Fig. 3 display the transverse momentum correlations when the detectors scan the Fourier plane in the perpendicular direction to the optical table (*x*-direction) for different postselected polarizations. Fig. 3(c) depicts $S(q_e^x;q_o^x)$, whereas Fig. 3(d) illustrates $S(q_o^x;q_e^x)$. From the graphs, it is clear that the vertical transverse correlation changes drastically with respect to the horizontal transverse behavior: The orientation of the coincidence rate shows a negative correlation, mainly due to the contribution of the walk-off angles, ρ_μ, only in the *x*-direction as can be seen by the term $\rho_e q_e^x \sin\phi_e$ in Eq. (3b) and the term $\rho_p\Delta_0-\rho_e q_e^x\cos\phi_e$ in Eq. (3c). Additionally, given that the walk-off affects only the *e*-photon, the polarizers play an important role, since when the *e*-photon arrives to detector *A* or when it arrives to detector *B*, the shape of the spatial mode function is different, as expected from the theory.

In conclusion, we have experimentally demonstrated that for a fixed value of the pump's waist, it is possible to achieve different kinds of transverse correlations between Type II SPDC photons by changing the direction in which the Fourier plane is scanned. Additionally, the correlation in the vertical direction is affected by the chosen postselection polarization scheme. These behaviors occur because of the crystal birefringence that results in a walk-off angle that affects the *e*- and *o*-photon differently and introduces a distinguishability between different directions of the transverse correlations that has to be taken into account if one is interested, for example, in the preparation of Bell states. Our results complement the already well-known methods in which the pump spatial and spectral profiles are used to tune the spatial correlations of SPDC photons.

Funding. Facultad de Ciencias, Universidad de los Andes.

Acknowledgment. The authors thank the discussions, contributions, and electronic technical support given by David A. Guzmán.

REFERENCES

1. A. Einstein, B. Podolsky, and N. Rosen, Phys. Rev. **47**, 777 (1935).
2. S. J. Freedman and J. F. Clauser, Phys. Rev. Lett. **28**, 938 (1972).
3. G. Scarcelli, A. Valencia, S. Gompers, and Y. Shih, Appl. Phys. Lett. **83**, 5560 (2003).
4. A. Valencia, G. Scarcelli, and Y. Shih, Appl. Phys. Lett. **85**, 2655 (2004).
5. D. V. Strekalov, A. V. Sergienko, D. N. Klyshko, and Y. H. Shih, Phys. Rev. Lett. **74**, 3600 (1995).
6. T. B. Pittman, Y. H. Shih, D. V. Strekalov, and A. V. Sergienko, Phys. Rev. A **52**, R3429 (1995).
7. M. D'Angelo, M. V. Chekhova, and Y. Shih, Phys. Rev. Lett. **87**, 013602 (2001).
8. V. Giovannetti, S. Lloyd, L. Maccone, and J. H. Shapiro, Phys. Rev. A **79**, 013827 (2009).
9. M. A. Nielsen and I. L. Chuang, *Quantum Computation and Quantum Information* (Cambridge University, 2011).
10. Y. H. Shih and C. O. Alley, Phys. Rev. Lett. **61**, 2921 (1988).
11. I. Marcikic, H. de Riedmatten, W. Tittel, V. Scarani, H. Zbinden, and N. Gisin, Phys. Rev. A **66**, 062308 (2002).
12. M. D'Angelo, Y.-H. Kim, S. P. Kulik, and Y. Shih, Phys. Rev. Lett. **92**, 233601 (2004).
13. P. G. Kwiat, K. Mattle, H. Weinfurter, A. Zeilinger, A. V. Sergienko, and Y. Shih, Phys. Rev. Lett. **75**, 4337 (1995).
14. Y. Shih, *An Introduction to Quantum Optics: Photon and Biphoton Physics* (CRC Press, 2011).
15. A. Migdall, S. Polyakov, J. Fan, and J. Bienfang, *Single-Photon Generation and Detection* (Academic, 2013).
16. R. Ramírez-Alarcón, H. Cruz-Ramírez, and A. B. U'Ren, Laser Phys. **23**, 055204 (2013).
17. G. Molina-Terriza, S. Minardi, Y. Deyanova, C. I. Osorio, M. Hendrych, and J. P. Torres, Phys. Rev. A **72**, 065802 (2005).
18. L. M. Procopio, O. Rosas-Ortiz, and V. Velázquez, Math. Models Methods Appl. Sci. **38**, 2053 (2015).
19. C. I. Osorio, G. Molina-Terriza, B. G. Font, and J. P. Torres, Opt. Express **15**, 14636 (2007).
20. S. Walborn, C. Monken, S. Pádua, and P. S. Ribeiro, Phys. Rep. **495**, 87 (2010).
21. M. Hamar, J. Peřina, O. c. v. Haderka, and V. Michálek, Phys. Rev. A **81**, 043827 (2010).
22. M. P. Edgar, D. S. Tasca, F. Izdebski, R. E. Warburton, J. Leach, M. Agnew, G. S. Buller, R. W. Boyd, and M. J. Padgett, Nat. Commun. **3**, 984 (2012).
23. E. Brambilla, A. Gatti, M. Bache, and L. A. Lugiato, Phys. Rev. A **69**, 023802 (2004).
24. R. Machulka, O. Haderka, J. Peřina, M. Lamperti, A. Allevi, and M. Bondani, Opt. Express **22**, 13374 (2014).
25. M. Ostermeyer, D. Korn, D. Puhlmann, C. Henkel, and J. Eisert, J. Mod. Opt. **56**, 1829 (2009).
26. S. Yun, P. Xu, J. S. Zhao, Y. X. Gong, Y. F. Bai, J. Shi, and S. N. Zhu, Phys. Rev. A **86**, 023852 (2012).
27. J. Flórez, O. Calderón, A. Valencia, and C. I. Osorio, Phys. Rev. A **91**, 013819 (2015).